
Article:
Evangelista, Danilo Elton, de Oliveira Arnoldi Pellegrini, Vanessa, Espirito Santo, Melissa et al. (3 more authors) (2019) Biochemical characterization and low-resolution SAXS shape of a novel GH11 exo-1,4-β-xylanase identified in a microbial consortium. APPLIED MICROBIOLOGY AND BIOTECHNOLOGY. pp. 8035-8049. ISSN: 0175-7598

https://doi.org/10.1007/s00253-019-10033-8

Biochemical characterization and low-resolution SAXS shape of a novel GH11 exo-1,4-β-xylanase identified in a microbial consortium

Danilo Elton Evangelista[1a], Vanessa de Oliveira Arnoldi Pellegrini[1a], Melissa Espirito Santo[1], Simon McQueen-Mason[2], Neil C. Bruce[2] and Igor Polikarpov[1*].

[1]Instituto de Física de São Carlos, Universidade de São Paulo, Avenida Trabalhador São-carlense 400, 13566-590 São Carlos – SP, Brazil.

[2]Department of Biology, University of York, Wentworth Way, York, UK, YO10 5DD

[a]These authors contributed equally to this work

*Correspondent author: ipolikarpov@ifsc.usp.br

ACKNOWLEDGEMENTS

The authors acknowledge Dr. Marco A. S. Kadowaki for his help with HPAEC analysis and Dr. Evandro Ares de Araújo for assistance with SAXS data collection and processing.

Abstract

Biotechnologies that aim to produce renewable fuels, chemicals, and bioproducts from residual ligno(hemi)cellulosic biomass mostly rely on enzymatic depolymerization of plant cell walls (PCW). This process requires an arsenal of diverse enzymes, including xylanases, which synergistically act on the hemicellulose, reducing the long and complex xylan chains to oligomers and simple sugars. Thus, xylanases play a crucial role in PCW depolymerization. Until recently, the largest xylanase family, glycoside hydrolase family 11 (GH11) has been exclusively represented by endo-catalytic β-1,4- and β-1,3-xylanases. Analysis of a metatranscriptome library from a microbial lignocellulose community resulted in the identification of an unusual exo-acting GH11 β-1,4-xylanase (MetXyn11). Detailed characterization has been performed on recombinant MetXyn11 including determination of its low-resolution small angle X-ray scattering (SAXS) molecular envelope in solution. Our results reveal that MetXyn11 is a monomeric globular enzyme that liberates xylobiose from heteroxylans as the only product. MetXyn11 has an optimal activity in a pH range from 6 to 9 and an optimal temperature of 50 ºC. The enzyme maintained above 65% of its original activity in the pH range 5 to 6 after being incubated for 72 h at 50 ºC. Addition of the enzyme to a commercial enzymatic cocktail (CelicCtec3) promoted a significant increase of enzymatic hydrolysis yields of hydrothermally pretreated sugarcane bagasse (16% after 24 h of hydrolysis).

Keywords: GH11 exo-β-1,4-xylanase; Metatranscriptome; Biochemical characterization; Synergism; Small Angle X-ray Scattering.

INTRODUCTION

Use of residual plant biomass as a feedstock for the production of biofuel, chemicals, and renewable materials, represents a feasible, sustainable and environmentally friendly alternative to fossil fuel-derived products (Isikgor and Becer 2015; Sims et al. 2010; Silva et al. 2018). Conversion of plant residues into these products relies on the controlled deconstruction and depolymerization of plant cell walls (PCW) (Keegstra 2010). Because of the intricate ultrastructure and diversified linkage complexity of PCW, efficient enzymatic processing of biomass-based feedstocks remains a challenge (Isikgor and Becer 2015; Johnson 2016; Silva et al. 2018). The enzymatic depolymerization of PCW is currently one of the most expensive technological steps in its valorization (Johnson 2016). Existing enzyme cocktails comprise mixtures of different plant cell wall degrading enzymes (PCWDE), each one with a distinct mechanism of action that synergistically reduce the PCW into simple sugars (Silva et al. 2018). Therefore, in order to decrease associated costs and increase efficiency, there is a constant demand for new enzymes with biochemical and biophysical properties that match industrial requirements, such as thermal and pH stability, activity at a broad pH range, and different substrate specificities or new mechanisms of activity, to list a few. Our current knowledge of enzymatic deconstruction of PCWs is incomplete and the discovery and characterization of new enzymes with novel catalytic mechanisms will contribute to a better understanding of PCW depolymerization.

Although PCWDE have been characterized from plants (Johansson et al. 2002; Suzuki et al. 2002) and animals (Evangelista et al. 2015; Watanabe and Tokuda 2001; Pauchet et al. 2010), microorganisms represent the main source for enzyme discovery. In this context, metatranscriptomic studies on complex unculturable microbial communities have greatly enhanced the pace of identification of enzymes from underexplored and uncultivable microorganisms (Castillo et al. 2013; Rittmann et al. 2006; Curtis et al. 2003; Duan and Feng 2010). For these reasons, we have conducted metatranscriptomic studies of a microbial consortium, which was grown in a nutrient-limited medium enriched with sugarcane bagasse, to selectively favor microorganisms capable of degrading PCW (Mello et al. 2016; Evangelista et al. 2018). In the course of these studies, a GH11 exo-acting β-1,4-xylanase, termed here MetXyn11, was identified (GenBank accession number: ATY75129.1).

Xylanases cooperatively act on xylan (the major component of hemicellulose), which is composed of a linear backbone chain of xylopyranose residues linked by β-1,4 glycosidic bonds and decorated with

β-D-galactopyranosyl, α-L-arabinofuranosyl, and α-D-glucuronic acid or its 4-*O*-methyl ether derivative residues (Pollet et al. 2010; Paës et al. 2012; Kalim et al. 2015; Biely et al. 2016). Due to their essential participation in biomass depolymerization, xylanases have been widely applied in several industrial sectors, such as second-generation bioethanol production; prebiotic production; pulp treatment; xylitol production; industrial waste treatment; and degumming of fibers for paper and textiles, to name a few (Kalim et al. 2015; Paës et al. 2012). Xylanases from GH10 and GH11 families are the most studied and widely used in biotechnological applications. In contrast to other GH families that comprise xylanases, GH11 is known as "true β-1,4-xylanase" family, because it is almost entirely composed of β-1,4-xylanases (Kalim et al. 2015; Paës et al. 2012). Moreover, until very recently, all GH11 members had been characterized as endo-catalytic enzymes that are highly specific for cleaving the internal linkages of the heteroxylans. However, our group recently identified the first GH11 with exo-β-1,4-xylanase activity (Mello et al., 2016).

Considering the essential role of xylanases in PCW depolymerization and biotechnological applications of these enzymes, here we report the identification and detailed characterization of a second GH11 family member (MetXyn11) that displays exo-β-1,4-xylanase activity, and demonstrate its ability to significantly increase sugar release when added to a commercial cellulase cocktail.

MATERIALS AND METHODS

Cloning, heterologous expression, and purification

MetXyn11was identified from a previously reported metatranscriptomic library (Mello et al. 2016; Evangelista et al. 2018). Its amino acid sequence was analyzed using BLASTP (Altschul et al. 1990), ExPASy (Wilkins et al. 1999), XtalPred (Slabinski et al. 2007) and SignalP 4.0 (Petersen et al. 2011) software. The MetXyn11 open reading frame (ORF), devoid of the signal peptide coding sequence, was cloned into the expression vector pETM11/LIC, using the ligation independent cloning (LIC) method (Camilo and Polikarpov 2014). First, the DNA sequence target was amplified by PCR, in which the genomic DNA extracted from the microbial consortia was used as a template. The following primers were designed to amplify MetXyn11 sequence (LIC tails are shown in italic): MetXyn11_Forward 5′-*CAGGGCGCCATG*GAACCCAAAATGCCACCTG-3′ and MetXyn11_Reverse 5′-*GACCCGACGCGG*TTAACGGGGTGTTTCATCCC-3′. The resulting plasmid was designed to express

MetXyn11 fused with a 6xHis-tag at the N-terminal region, including a cleavage site for *Tobacco etch* virus protease (TEV) between the two sequences (Camilo and Polikarpov 2014). This allows the proteolytic 6xHis-tag removal after the protein purification by Ni^{+2} affinity chromatography. The resulting plasmid was propagated in *Escherichia coli* (DH5α) cells (Thermofischer, Waltham USA), and the purified plasmid was used in the heat-shock transformation of *E. coli* Rosetta (DE3) cells (Novagen, Watertown USA) to create the MetXyn11 expression strain.

MetXyn11 expression was carried out in LB medium at 37 ºC for 5 h ($O.D._{600} = 0.6$), followed by an induction step at 18 ºC for 24 h, containing 1 mM IPTG. The cells were pelleted at 2.500 *x g* for 45 min at 4 ºC, suspended in lyses buffer (50 mM Tris pH 8.0, 150 mM NaCl, 4 mM PMSF, 2 mM DTT, 10% (v/v) glycerol and 50 $\mu g.mL^{-1}$ of lysozyme), incubated at 18 ºC for 20 min and sonicated on an ice bath using a 550 Sonic Dismembrator Sonifier (Fisher Scientific, Hampton USA). Next, the cells were pelleted (6,000 *x g*, 45 min at 4 ºC) and the supernatant was used for MetXyn11 protein purification.

Three chromatographic steps were used for MetXyn11 purification: two steps of Ni^{+2} affinity chromatography, one before and one after TEV proteolysis; and a third step of size exclusion chromatography. In the first step, MetXyn11 (~30 kDa) attached to 6xHis-tag was eluted using 50 mM Tris pH 8.0, 150 mM NaCl and 125 mM imidazole. The sample was dialyzed to remove traces of imidazole and then, incubated with 3 $mg.mL^{-1}$ of TEV protease at 4 ºC for 48 h. In the second purification step, MetXyn11 (~29 kDa) free of 6xHis-tag was eluted in 50 mM Tris pH 8.0 and 150 mM NaCl. The third purification step was conducted on a Superdex^{TM} 75 prep grade 16/60 (GE-Healthcare, Chicago USA) gel filtration column equilibrated with 50 mM Tris pH 8.0 and 150 mM NaCl. The protein was concentrated to 1 $mg.mL^{-1}$, using the 10 kDa Vivaspin Concentrator (GE-Healthcare, Chicago USA) at 1,500 *x g* and stocked at 4 ºC. The protein integrity and sample purity were confirmed by the 15% SDS-PAGE (sodium dodecyl sulfate–polyacrylamide gel electrophoresis) analysis.

Thermofluor assays

To determine the best condition for the enzyme storage and handling, the enzyme's thermal stability was evaluated using in several different buffered solutions using a thermal shift fluorescence (Thermofluor) assay (Table S1, Supplementary Materials). Moreover, we also assessed the MetXyn11 tertiary structure stability in different pH conditions, using the 50 mM sodium acetate/ borate/ phosphate (ABF) buffer in a pH range from pH 2 to 10. The experiments consisted of 20 µL reaction containing 13 µM of the enzyme

in 50 mM buffer with 5 µL of SYPRO Orange dye 10X (Invitrogen, Carlsbad USA). Reactions were performed in triplicate in a 96-well thin-wall PCR plate (Bio-Rad, Hercules USA). The plate was sealed with Optical-Quality Sealing Tape (Bio-Rad, Hercules USA), then incubated in an iCycler iQ Real-Time PCR Detection System (Bio-Rad, Hercules USA). The temperature ranged from 25 to 90 ºC, increasing 1 °C per minute, added of a holding step of 30 seconds at each point. The extrinsic fluorescence from the probe was measured at 490/530 nm of excitation/emission wavelengths. The melting temperature (T_m) was calculated by Boltzmann sigmoidal function, using the GraphPad Prism 6.0 software (GraphPad Software Inc., La Jolla USA).

Enzymatic assays

The MetXyn11 enzymatic activity was quantified by the DNS method that measures the reducing end-groups of saccharides (Miller 1959). All experiments were conducted in triplicate. Enzyme specificity was assessed using 15 different substrates: Avicel, carboxymethylcellulose, Sigmacell20 and hydroxyethylcellulose (all from Sigma, St. Louis USA); glucuronoxylan from beechwood; arabinoxylan from rye flour, arabinan, debranched arabinan, β-glucan, xyloglucan, dextrin, galactomannan, larch arabinogalactan, lichenan and mannan (all from Megazyme, Bray, Republic of Ireland). Since MetXyn11 showed significant activity only against glucuronoxylan, this substrate was used for the subsequent biochemical experiments. The reaction consisted of 35 nM of enzyme mixed with 1% (w/v) glucuronoxylan and 50 mM buffer ions in 50 µL final volume, which was incubated for 10 min. The reaction was stopped by the addition of 100 µl of DNS reagent and heating at 95 ºC for 10 min, followed by cooling on ice for 1 min for color stabilization. Product absorbance was measured at 540 nm using the MultiSkan Spectrum equipment (Thermo Scientific, Waltham USA), and a standard concentration curve of D-(+)-xylose (Sigma, St. Louis USA) was used to express results in reducing sugars equivalents. All the obtained data were analyzed using the GraphPad Prism 6.0 software (GraphPad Software Inc., La Jolla USA).

The optimum pH was evaluated in pH range from 2 to 10 in ABF buffer at 50 ºC. The optimal temperature was assessed in a potassium phosphate buffered solution at 50 mM concentration and pH 7.0 in a temperature range from 30 to 70 ºC. In both sets of experiments the reactions were performed as described above. Moreover, enzyme stability assays were performed, quantifying MetXyn11 residual activity after enzyme pre-incubation under long periods in different temperatures or pHs. During the thermal stability assays MetXyn11 was kept at 50 ºC in potassium phosphate buffer pH 6.0 for 120 h. For

157 the pH stability assay, MetXyn11 was maintained in ABF buffer at pH range from 2 to 10 at 50 ºC for 72
158 h. The residual activity was measured under the optimal temperature and buffer conditions. Furthermore,
159 under the optimal conditions, the enzyme activity was also evaluated upon addition of 15 different chemical
160 compounds (Table S2, Supplementary Materials). To evaluate enzyme kinetics, the reactions were
161 performed under the optimal conditions enzymatic activity, varying glucuronoxylan concentration from 0.1
162 to 18 $mg.mL^{-1}$

163 **Enzymatic cleavage pattern determined by high-performance anion exchange chromatography**
164 **(HPAEC)**

165 The soluble products released by the MetXyn11 catalytic action on heteroxylans (glucuronoxylan and
166 arabinoxylan) and on xylohexaose were analyzed using HPAEC. In experiments with heteroxylans,
167 reactions containing 1% of substrate and 35 nM of MetXyn11 were conducted under optimal conditions
168 for 24 h. For comparison, we also performed experiments using a typical endo-1,4-β-xylanase
169 (rGH11Xyn11B; Ghio et al. 2017) instead of MetXyn1, to compare their heteroxylan cleavage pattern. In
170 the experiments with xylohexaose, the reactions were conducted with 55 μM of substrate and analyzed in
171 1, 5, 10 and 15 min time points. A pool containing 5 μL of each reaction conducted in triplicate was diluted
172 10-fold, then centrifuged at 13,000 *x g* for 5 min and the supernatant was analyzed by a DIONEX ICS3000
173 instrument (DIONEX, Sunnyvale USA) connected to a CarboPac PA1 4 X 250 mm column (DIONEX,
174 Sunnyvale USA). The column was equilibrated with 100 mM NaOH at 1 $mL.min^{-1}$ for 5 min; the sugars
175 were separated using a gradient from 100 mM NaOH/0 mM NaAc to 100 mM NaOH/150 mM NaAc over
176 20 minutes.

177 **Supplementation of commercial enzymatic cocktail for pretreated plant biomass saccharification**

178 Hydrothermally pretreated sugarcane bagasse was used in saccharification assays with Celic CTec3 ±
179 MetXyn11. The biomass was provided by the Raízen Group (Costa Pinto/Piracicaba, São Paulo, Brazil).
180 The raw material was rinsed with hot water (50 °C ± 5 °C) and milled using a knife mill. Next, it was dried
181 in the oven at 60 °C for 24 h and hydrothermally pretreated.

182 Hydrothermal pretreatment was performed using hot water for 30 minutes at 160 °C in a pretreatment
183 reactor AU/E-20 model (Regmed, Osasco Brazil). The pressure was kept at 7 bar and a 1:10 solid to liquid
184 ratio (grams of bagasse/mL of water) was used (Santo et al. 2018). The pretreated sugarcane bagasse used
185 in the study contained 76.8% ± 1.5% of glucan, 6.1% ± 0.1% of xylan, 17.8%± 0.5% of lignin and 1.4% ±

186 0.02% of ash content. The saccharification of pretreated sugarcane bagasse was carried out at a substrate
187 concentration of 10% (w/v). Cellic CTec3 (Novozymes, Kalundborg DKK) protein loading was 5 mg/g of
188 substrate in the control reactions. To evaluate effect of MetXyn11 supplementation 0.125 mg of the enzyme
189 per g of substrate was added to Cellic CTEc3 reaction. The reactions were conducted in a citrate buffer (50
190 mM, pH 5.0), at 50 °C up to 72 h. The soluble hydrolysate products were analyzed by high performance
191 liquid chromatography (HPLC) (Shimadzu, Kyoto Japan), equipped with refractive index detector and UV-
192 VIS spectrophotometer. Aminex HPX-87 H (Bio-Rad, Hercules USA) column was used and 5 mM H_2SO_4
193 solution at 65 °C was utilized as a mobile phase (flow rate 0.6 $mL.min^{-1}$). Glucose and xylose were used as
194 standards.

195 **Homology modelling of MetXyn11**

196 A multiple alignment was performed, using T-Coffe Server (Notredame et al. 2000), for comparative
197 analyses between MetXyn11 amino acid sequence and some of the traditional GH11 endo-β-1,4-xylanases,
198 and also Compost21_GH11 enzyme, that represents the unique previously reported GH11 exo-β-1,4-
199 xylanase (Mello et al. 2016). Moreover, a three-dimensional (3D) homology model of MetXyn11 was
200 generated using the MetXyn11 amino acid sequence and using the Compost21_GH11 crystal structure
201 (PDB id: 5VQJ) as inputs in the I-Tasser software (Yang et al. 2015). Following this, the 3D homology
202 model was superimposed with the crystal structures of the GH11 members used in our amino acid sequences
203 alignment, using Pymol program (DeLano 2002)

204 **SAXS studies**

205 Small angle X-ray scattering (SAXS) experiments were carried out at the D02A-SAXS1 beamline of
206 the Brazilian Synchrotron Light Laboratory (LNLS, Campinas, Brazil). To remove protein aggregates,
207 samples (at the concentrations of 1, 7.5 and 15 $mg.mL^{-1}$ in 50 mM potassium phosphate pH 7.0 and 150
208 mM NaCl) were centrifuged at 17,000 *x* g for 5 min at 4 °C prior to measurements, and the supernatant was
209 collected. Next, the supernatant was loaded in a 1 mm path-length capillary cell and exposed to X-rays
210 during 10 frames of 30 s, with intervals of 1 s between each frame. The data sets were collected using a
211 monochromatic X-ray beam (λ= 1.55 Å) with a Pilatus 300 area detector (Dectris, Baden Switzerland). To
212 cover a scattering vector ($q=4\pi/\lambda\sin(\theta)$, being 2θ the scattering angle) range from 0.012 to 0.400 $Å^{-1}$, the
213 distance between sample and detector was adjusted to ~1,000 mm. The scattering from buffer alone was
214 subtracted from the sample`s scattering. Comparative analysis between each frame was used to verify

radiation damage. Guinier analysis (Guinier and Fournet 1955; Konarev and Svergun 2015; Perry and Tainer 2013) was applied to verify monodispersivity and to calculate the radius of gyration (R_g), which was also estimated by an indirect Fourier transform method, using the GNOM program (Svergun 1992). The distance distribution function P(r) was analyzed by GNOM and the maximum particle dimension (D_{max}) was determined. Ten ab initio envelope models were generated by DAMMIN (Franke et al. 2009), then aligned and averaged by DAMAVER (Volkov and Svergun 2003), to build the final MetXyn11 molecular envelope. The 3D-homology model of MetXyn11 structure was inputted into Crysol online software (Svergun et al. 1995) to generate a theoretical SAXS profile, which was compared to the experimental SAXS profile. Moreover, the 3D-homology model of MetXyn11 structure and the final model of MetXyn11 molecular envelope were superimposed by SUPCOMB program (Kozin and Svergun 2001).

RESULTS

Bioinformatic analysis

Bioinformatic analysis revealed that MetXyn11 has 268 amino acid residues (including a putative 21-residue signal peptide) and a molecular mass of ~28 kDa. The enzyme has a calculated isoelectric point of 6.22. MetXyn11 has the highest amino acid sequence similarity (id > 80%) with Compost21_GH11 (PDB id: 5VQJ) and another GH11 exo-β-1,4-xylanase (GenBank: ATY75130.1), identified in the same metatranscriptomic library. The organism(s) that carries (carry) these exo-β-1,4-xylanase genes is(are) still unknown, however, MetXyn11 also shows high similarity to other known GH11 endo-β-1,4-xylanase from bacterial sources, particularly with the enzymes from the *Cellvibrio* genus including *Cellvibrio* sp. PSBB006, *Cellvibrio mixtus*, *Cellvibrio* sp. PSBB023 and *Cellvibrio* sp. pealriver (all with id = 78%).

Comparative analyses between the amino acid sequences and 3D structures of MetXyn11, Compost21_GH11 and some typical GH11 endo-β-1,4-xylanases revealed some notable differences between these enzymes (Fig. 1). The first noticeable difference between these enzymes is the extended amino acid sequence at the N-terminus of MetXyn11, which was predicted as being an extra α-helix. The second difference between these enzymes, is the two extra loops shared by MetXyn11 and Compost21_GH11, which are absent in typical GH11 endo-β-1,4-xylanases.

Cloning, heterologous expression and purification

MetXyn11 ORF was cloned into the pETM11/LIC expression vector, and used to transform *E. coli* Rosetta cells. The enzyme was successfully overexpressed as a soluble protein fused to the 6xHis-tag (Fig. 2). The enzyme was purified in three purification steps and eluted as a single peak after size exclusion chromatography, confirming sample purity. The MetXyn11 molecular mass estimated by SDS-PAGE (~28 kDa) is in agreement with the theoretical molecular mass predicted from its amino acid sequence (Fig. 2).

Substrate specificity and hydrolytic products

MetXyn11 specific activity was tested against 15 different plant polysaccharides. Among all the tested potential substrates, the enzyme showed detectable enzymatic activity only against glucuronoxylan and arabinoxylan. MetXyn11 has a much higher activity for glucuronoxylan than to arabinoxylan. Indeed, as evaluated by the DNS method, MetXyn11 exhibited a 50 times lower specific activity for arabinoxylan when compared to glucuronoxylan. To evaluate the products released by MetXyn11 on these substrates, we analyzed them using HPAEC-PAD (Fig. 3). For both substrates, the enzyme released xylobiose as the unique product, indicating an exo catalytic pattern. For comparison both substrates were also hydrolysed by *Paenibacillus* sp. A59 GH11 endoxylanase (rGH11XynB; Ghio et al., 2018) kindly donated by Prof. Eleonora Campos (INTA, Argentina), revealing strikingly different hydrolytic patterns. Liberation of xylobiose by MetXyn11 was also confirmed by the experiments using xylohexaose as a substrate (Fig. 4). In these experiments, the profile of xylo-oligosaccharides evaluated over the 15 min of reaction revealed the conversion of xylohexaose into xylotetraose plus xylobiose, then, the conversion of xylotetraose to xylobiose. Since the xylohexaose used here had a small amount of xylopentaose contamination (Fig. S1, Supplementary Materials), it was also possible to observe the conversion of the xylopentaose in xylotriose plus xylobiose.

Optimal conditions for MetXyn11 stability

Optimal conditions for MetXyn11 stability were determined by assessing its tertiary structural integrity in several different buffer solutions at different temperatures by Thermofluor analysis (Ericsson et al. 2006) (Table S1, Supplementary Materials). The results showed a good fit with the Boltzmann sigmoidal equation, which is usually applied for non-linear fitting of thermal denaturation data, revealing that MetXyn11 tertiary structure has a T_m value of 55 ^oC in its best buffer conditions (Fig. 5). MetXyn11 is most stable between pHs 5.5 and 7.0, in sodium phosphate pH 5.5, MES pH 5.8-6.5, Bis-Tris pH 6.0-7.0 and HEPES pH 7.0 (T_m = 55 ^oC) buffers, followed by several other buffers with pHs between 4.7 and 8.5

(T_m = 51-54 °C). The enzyme was least stable at the extreme pHs: HCl pH 2.0 (T_m = 26 °C), citric acid pH 3.0 (T_m = 46 °C) and sodium carbonate pH 9.5-10.0 (T_m = 46 °C).

Effects of metal ions and chemicals on enzyme activity

MetXyn11 activity was evaluated in the presence of different metal ions and chemicals (Table S2, Supplementary Materials). The major detrimental effects were observed for SDS (sodium dodecyl sulfate) and Fe^{+3} that completely inactivated the enzyme, followed by Mn^{+2}, Fe^{+2}, Cu^{+2}, Co^{+2} and Ca^{+2} which imparted a loss of approximately 78%, 46%, 46%, 21% and 20% of its catalytic activity, respectively. In contrast, Li^{+2}, Ni^{+2}, K^{+} and Mg^{+2} enhanced MetXyn11 activity by approximately 6%, 10%, 12% and 23%, respectively. Neutral surfactants, Tween-20 and Triton-100X respectively provoked a loss of 16.5 % and a gain of 8% on MetXyn11 activity, respectively. The reducing agents DTT and β-mercaptoethanol caused decrease of the enzyme activity equal to 15% and 5%, respectively.

MetXyl11 optimal activity and the enzyme kinetics

MetXyn11 activity was highest around 50 °C; however, the enzyme maintained over 80% of its optimal activity at both 40 °C and 60 °C (Fig. 6A). We also determined the MetXyn11 activity profile following variations of pH. The enzyme showed the best performance at pH 6-7, retaining above 60% of the maximum activity at pH 5, approximately 90% at pH 8-9 and 80% at pH 10. No significant activity was detected at pHs below 5 (Fig. 6B). According to the BRENDA database (Schomburg et al. 2017), the optimal temperature of GH11 xylanases (derived from several distinct microorganisms) varies from 22 to 90 °C and the optimal pH from 2 to 11. However, most of these enzymes have an optimal activity between 40 and 65 °C and pH 4-7. Therefore, the MetXyn11 activity profile is consistent with those of most of GH11 xylanases. Kinetics assays were performed under the enzyme optimal conditions, using glucuronoxylan as a substrate (Fig. 6C). Interestingly, the reactions revealed a "first-order reaction" profile even at 18 mg/L of substrate. Nevertheless, based on the data obtained predicted values of V_{max} =50.30 $\mu M.s^{-1}$, K_M of 121 $mg.mL^{-1}$, k_{cat} of 1437 s^{-1} and a catalytic efficiency (k_{cat}/K_M) of 11.88 $mL.s^{-1}.mg^{-1}$, respectively, were obtained using GraphPad Prism 6.0 software (GraphPad Software Inc., La Jolla USA). The obtained K_M is consistent with a very poor binding of the enzyme to insoluble substrate (glucuronoxylan). A high K_M value offsets an elevated turnover number, resulting in a low catalytic efficiency of the enzyme on glucuronoxylan.

300 **Thermal and pH stability of MetXyn11**

301 MetXyn11 stability was evaluated both as a capacity to maintain the enzyme fold and a capacity
302 to maintain its catalytic activity. For the former, we used Thermofluor analyses, in which MetXyn11 was
303 exposed to a wide pH range during a linear increment on temperature until its thermal denaturation. The
304 results show a signal from the fluorescence probe detected at the beginning of the experiment at pH 2,
305 indicating enzyme denaturation (Fig. 5B). At pH 3, the MetXyn11 structure exhibited a low T_m value of 34
306 ^oC, increasing to 44 ^oC at pH 4 until the maximum value of 52 ^oC at pH 6, and then discretely decreasing
307 until 43 ^oC at pH 10 (Fig. 5B). Furthermore, residual activity of MetXyn11 was measured during 120 h
308 under the optimal conditions for its enzymatic activity (Fig. 5C). MetXyn11 maintained almost 80% of its
309 original activity after being incubated for 24 h, followed by 67%, 65%, 45% and 20%, respectively, after
310 48 h, 72 h, 96 h and 120 h. MetXyn11 residual activity was also measured after 72 h at optimal temperature,
311 but varying the pH from 2 to 10 (Fig. 5D). MetXyn11 presented no significant residual activity for pHs 2
312 and 3. At pH 4, MetXyn11 retained 14% of its initial activity, about 70% at pH 5-6, 40% at pH 7, followed
313 by a gradual decrease to 18% at pH 10.

314 **Enhancement of biomass hydrolysis by MetXyn11 supplementation to commercial enzymatic**
315 **cocktail**

316 To test the capacity of MetXyn11 to enhance biomass hydrolysis by a commercial enzymatic
317 cocktail, we hydrolysed pretreated sugar cane bagasse using Cellic CTex3 alone and also supplemented by
318 MetXyn3. Although MetXyn11 action alone did not lead to any detectable levels of released xylose or
319 glucose, the enzyme addition to Cellic CTec3 led to a significantly enhanced hydrolytic activity of the
320 cocktail on sugarcane bagasse as compared with the Cellic CTec3 alone. The levels of cellulose hydrolysis
321 achieved in 24 h, 48 h, and 72 h, were 46.9%, 59,4%, and 63.3% respectively compared to Cellic CTec3
322 alone, while they reached 54.5%, 67%, and 68.7% when Cellic CTec3 was combined with MetXyn11 (Fig.
323 7A). Corroborating with the literature (Väljamäe et al. 1999; Boisset et al. 2001; Pellegrini et al. 2018), the
324 relative increase in the hydrolysis yields was higher at the beginning of the reaction (at 24 h an increase in
325 cellulose conversion was 16.6%) whereas at 48 h and 72 h the observed gains were 13.3%, and 8.6%. (Fig.
326 7B). Levels of xylan hydrolysis, which reached 51.5%, 59.5% and 64% in 24 h, 48 h and 72 h using Cellic
327 CTec3 alone, were increased to 53.9%, 62.2% and 66.7% when Cellic CTec3 was supplemented by

MetXyn11 (Fig. 7C&D). Thus, MetXyn11 addition provoked a significant increase of enzymatic hydrolysis of pretreated sugarcane bagasse when used in combination with Celic CTec3.

Low resolution shape of MetXyn11 in solution

SAXS studies were performed to determine the MetXyn11 low-resolution molecular envelope in solution. Structural parameters, data plot curves and the molecular envelope model obtained from SAXS experiments are summarized in Table S3 (Supplementary Materials), Figs. 8 and 9. Analysis of the initial *q*-region of the scattering curves using Guinier approximation (*lnI(q) versus* q^2) exhibits the linear correlation expected for monodisperse samples, indicating homogeneity of the particles in solution (Fig. 8A). In addition, the calculated R_g (18.52 Å) from each scattered frame remained constant (within the experimental errors) along the different protein concentrations, indicating: first, an absence of radiation damage and, second, an absence of attractive or repulsive interactions between the particles.

The distance-distribution p(r) plot has an almost perfect bell-shape, which is characteristic of well-defined spherical particles, but the curve also shows an extended tail with a small second peak at the highest *q*-region (Fig. 8B), indicating that MetXyn11 might have a small module that protrudes from the overall globular shape (Perry and Tainer 2013). Moreover, D_{max} and R_g of MetXyn11 are equal to, respectively, 58 Å and 17.67 Å, which is similar to the data obtained from Guinier analysis. The Porod-Debye plot (q^4 *x I(q) versus* q^4) displays a clear plateau, which is consistent with the observation that MetXyn11 is a globular-like protein that lacks disordered regions (Fig. 8C) (Perry and Tainer 2013; De Oliveira et al. 2015; Rambo and Tainer 2011). The dimensionless Kratky curve (q^2 *x I(q) versus q*), which provides a notion about the degree of the particle compactness, has a well-defined maximum very close to 1.1 at $qR_g = 1.6$. That is, again, coherent with a nearly globular protein in solution (Fig. 8D) (Rambo and Tainer 2011; Perry and Tainer, 2013). Furthermore, at $qR_g > 6$ there is a subtle elevated baseline, suggesting that MetXyn11 may exhibit some degree of flexibility (Perry and Tainer 2013; De Oliveira et al. 2015). All the experimental SAXS data fitted well to the theoretical SAXS plots generated from the 3D-homology model of MetXyn11 structure. Finally, the low-resolution envelope snugly fits the 3D-homology model of the MetXyn11, revealing a monomeric globular-like protein with a protuberance at its N-terminus (Fig. 9).

DISCUSSION

A novel GH11 xylosidase

Substrate specificity assays using different plant polysaccharides revealed that MetXyn11 exhibited activity only on glucuronoxylan and arabinoxylan. These results are in line with the previous observations since all known GH11 members are specific towards heteroxylans. Indeed, GH11 xylanases are considered to be "true" β-1,4-xylanases as compared to the other GH families (Pollet 2010; Paës et al. 2012), which are frequently able to act on different polysaccharides in addition to heteroxylans. For example, there are known bifunctional xylanases from GH16, GH43 and GH62 that have two distinct catalytic domains, one with xylanase activity, while the other having glucanase activity (for GH16) or arabinase activity (for both GH43 and GH62) (Paës et al. 2012). Moreover, GH5, GH8, GH10, and GH30 xylanases, which have a unique catalytic domain, show more versatility than members of the GH11 family. Some GH5 enzymes are specific for heteroxylans, however the GH5 family also includes cellulases, glucanases and mannanases (Pollet et al. 2010; Cantarel et al. 2009; Lombard et al. 2013). The same applies for the GH8 family, with a substitution of glucanases and mannanases for chitosanases and licheninases (Pollet et al. 2010; Cantarel et al. 2009; Lombard et al. 2013). The GH30 family contains both glucanases and galactanases (Cantarel et al. 2009; Lombard et al. 2013). Finally, the GH10 family mostly comprises endo-β-1,4-xylanases, with a few examples of endo-β-1,3-xylanases and β-1,4-xylosidases. Furthermore, GH10 enzymes can hydrolyze some glucose-derived substrates such as aryl-cello-oligosaccharides (Pollet et al. 2010).

The much lower activity of MetXyn11 towards arabinoxylan as compared to glucuronoxylan could be explained by a difference in the substrate´s decorations. Glucuronoxylan used in our experiments is only ~13% decorated by glucuronic acid, while arabinoxylan is ~40% decorated with arabinose residues. It is well known that GH11 xylanases have a narrow catalytic cleft unable to accommodate and cleave branched substrates (Pollet et al. 2010; Paës et al. 2012), which could explain MetXyn11 preference for glucuronoxylan as compared to arabinoxylan.

Quite remarkably though, despite having a profile of substrate specificity considered common among all GH11 endo-β-1,4-xylanases, MetXyn11 revealed an uncommon pattern of hydrolytic products (Fig. 3 and Fig. 4). Typical GH11 endo-β-1,4-xylanases release both xylobiose and xylotriose as main undecorated products from heteroxylans (Biely et al. 2016; Pollet et al. 2010). In addition, GH11 family

385 members also generate longer xylooligosaccharides (such as xylotetraose) linked to aldopentauronic acid
386 or by L-arabinofuranosyl residue at the penultimate xylopyranosyl residue from the non-reducing end as
387 their major decorated products released from glucuronoxylan and arabinoxylan, respectively (Biely et al.
388 2016). In contrast, our HPAEC analyses identified xylobiose as the unique product released by MetXyn11
389 both from glucuronoxylan and arabinoxylan, which is characteristic with its exo-catalytic activity (Fig. 3).
390 Furthermore, our HPAEC results clearly show a conversion of xylohexaose into xylotetraose plus
391 xylobiose, xylotetraose in xylobioses, and xylopentaose in xylotriose plus xylobiose. These results indicate
392 that MetXyn11 cleaves off terminal xylobiose molecules from xylooligosacharides and, also heteroxylans.

393 Our results are perfectly in line with the only other reported GH11 exo-β-1,4-xylanase
394 (Compost21_GH11) (Mello et al. 2017). The Compost21_GH11 hydrolysis of glucuronoxylan and
395 xylooligosaccharides also revealed xylobiose as a unique product liberated by the enzyme. The crystal
396 structure of Compost21_GH11 (PDB: 5VQJ) has the typical β-jelly-roll fold shared by all the other 32
397 GH11 xylanase structures deposited in PDB. However, Compost21_GH11 has two extra loops not present
398 in the other family members (Fig. 1B). These two extra loops are very close to the cleft and one of them
399 clearly blocks part of the catalytic groove, evidencing its contribution for the uncommon exo-catalytic
400 mechanism. Amino acid sequences alignment between MetXyn11 and Compost21_GH11 (Fig. 1A)
401 revealed that MetXyn11 also presents the two extra loops, which was also confirmed by the 3D
402 superposition between the crystal structure of Compost21_GH11 and the 3D-homology model of the
403 MetXyn11 structure (Fig. 1C). Therefore, a MetXyn11 exo-catalytic mechanism could be mediated by the
404 presence of these two extra loops.

405 Finally, our enzymatic kinetics results are consistent with the structural determinants of MetXyn11
406 (Fig. 6). A typical narrow cleft of all GH11 family enzymes decorated with two uncommon extra loops
407 (that might mediate MetXyn11 action as an exo-xylanase) significantly restrict MetXyn11 binding and
408 recognition of heteroxylans. This could explain why MetXyn11 kinetics display a "first-order reaction"
409 profile (as expected for very low concentrations of substrate binding-sites) even at high concentrations of
410 glucuronoxylan.

411 **Molecular shape of MetXyn11**

412 The analyses of amino acid sequence, SDS-PAGE, 3D-homology model and SAXS data provided
413 important information about the size, shape, compactness, and flexibility of MetXyn11. These data show

414 that MetXyn11 is a monomeric globular-like enzyme of ~28 kDa, with a β-jelly-roll fold and a high degree
415 of compactness, R_g between 17.6 and 18.5 Å and D_{max} close to 58 Å. These results are consistent with other
416 GH11 xylanases from a wide diversity of microorganisms, as reviewed by Paës and collaborators on the
417 basis of comparison of the biochemical and biophysical properties of 164 GH11 enzymes (Paës et al. 2012).
418 This paper shows that xylanases uniquely formed by the catalytic module are dense globular proteins with
419 molecular masses between 18 and 31 kDa, which have the same β-jelly-roll fold. Moreover, SAXS studies
420 of a 21-kDa enzyme from *Trichoderma longibrachiatum* showed R_g and D_{max} close to 17 Å and 50 Å,
421 respectively (Kozak 2006). As suggested by several authors, a relative small size and compactness of GH11
422 xylanases facilitate their penetration into the inner part of PCW, consequently, indicating that these
423 enzymes might initiate the PCW deconstruction, thus favoring consecutive action of larger enzymes (i.e
424 multi-domains enzymes) (Paës et al. 2012; Beaugrand et al. 2005).

425 Despite having the β-jelly-roll fold (two twisted antiparallel β-sheets and a single α-helix,
426 resembling the shape of a partially closed right hand) that is traditional for all GH11 enzymes, our 3D-
427 homology model and SAXS data revealed an unusual extra α-helix at the MetXyn11 N-terminus, which is
428 not present in all the 33 GH11 xylanases deposited in PDB, including the Compost21_GH11. This α-helix
429 has a considerable degree of flexibility, as suggested by the Kratky plot, and promotes a clear protuberance
430 at the N-terminal region of the MetXyn11 molecular envelope. The role of the additional α-helix is not yet
431 clear, thus requiring further experimental studies.

432 **Possible biotechnological applications for MetXyn11**

433 As aluded to above, xylanases, especially those from GH10 and GH11 families, have a wide range
434 of industrial applications (Polizeli et al. 2005; Kalim et al. 2015; Biely et al. 2016). The ability of
435 MetXyn11 to liberate xylobiose as the only soluble product might be advantageous for pre- and pro-
436 biotic formulations. Xylo-oligosaccharides find applications in the food sector due to their health benefits
437 and some biochemical characteristics which are considered advantageous when compared to other oligo-
438 saccharides. For example, xylo-oligosaccharides are stable over a wide pH range (2.5-8.0) and also at
439 temperatures up to 100 °C, in contrast to others non-digestible oligosaccharides such as fructo-
440 oligosaccharides, for example, that are unstable at the human gastric acid pH (Vazquez et al. 2000; Kumar
441 et al. 2012). Furthermore, xylobiose has a higher antifreeze activity than glucose, sucrose and maltose, and
442 also has a water activity similar to that shown by glucose (Vazquez et al. 2000; Kumar et al. 2012). Besides,

xylobiose is not carcinogenic, has acceptable odor and low calories, which favors its use in diet products formulation (Vazquez et al. 2000; Kumar et al. 2012).

In addition, MetXyn11 has the highest specific activity around 50 ºC, and also presents good stability at this temperature for 72 h or longer. These are important enzymatic properties for industrial applications, since temperatures close or above 50 ºC are usually required in the processing of complex polysaccharides to reduce its high viscosity and also help to prevent the undesirable growth of mesophilic contaminants (Kozak 2006). Moreover, MetXyn11 has a wide pH range of activity (pH 5-10), demonstrating high stability (70%) between pHs 5 and 6 after 72 h at 50 ºC. These results suggest that MetXyn11 could be used both in the processes that require alkaline pHs (i.e pulp and paper biobleaching) (Walia et al. 2017) and also in the processes which need acid pHs (i.e fruit juice and wine preparation) (Beaugrand et al. 2005).

Finally, MetXyn11 could be used as a complement of commercial enzymatic cocktails aiming for better yields of plant biomass enzymatic hydrolysis, as demonstrated by our Cellic CTec3 complementation experiments. MetXyn11 supplementation not only enhances levels of xylan hydrolysis, but also considerably increases levels of cellulose hydrolysis by Cellic CTec3 cellulases (Fig. 7). It is known that that Cellic CTec3 has endo-β-1,4-xylanase and β-xylosidase acitivities (Sun et al 2015; Hu et al 2016). It may be expected that xylobiose generated by the exo-xylanase is hydrolyzed into xylan as well as that primary sugarcane bagasse xylan hydrolysis products generated by the xylanase activity of Cellic CTec3 are subsequently shortened by exo-xylanase activity of MetXyn11, resulting in the enhance of hemicellulose hydrolysis. It was shown that the xylan polymer can bind tightly to the hydrophilic surfaces of the cellulose crystallites 2_1-fold helical screw conformation within the plant cell wall, thus significantly interfering with the cellulose enzymatic hydrolysis (Busse-Wicher et al 2014). Furthermore, pretreatment solubilized hemicellulose oligomers partly aggregate on the cellulose surfaces and physically block access of cellulases on the cellulose fibres (Kabel et al. 2007; Kumar et al. 2018). Moreover, solubilized fragments of the xylan backbone (xylooligosaccharides, XOS) and mixed-linkage β-glucans are strong inhibitors of cellulases (Kont et al 2013). Therefore, it was shown that β-xylanase supplementation increases cellulose hydrolysis in xylan-containing lignocellulosic materials (Zhang et al. 2011; Kont et al 2013; Sun et al 2015; Kumar et al 2018). Here we demonstrated that MetXyn11 supplementation of Cellic CTec3 leads to a significant increase in rates and yields of cellulose and xylan conversion from pretreated lignocellulosic biomass.

Final considerations: MetXyn11 is an unusual GH11 β-1,4-xylosidase

Our current work supports an importance of metatranscriptomic approaches for discovering novel and unusual enzymes that are not accessible by the traditional approaches of microbial cultivation in pure cultures, as so far, MetXyn11 is the second reported GH11 enzyme with a exo-β-1,4-catalytic mechanism. Homology modeling and amino acid sequence comparison indicate that the same two extra loops already described for the first reported GH11 exo-β-1,4-xylanase (Compost21_GH11) are also present in MetXyn11. In addition, MetXyn11 has an extra N-terminus α-helix which does not exist in other GH11 enzymes deposited in PDB, including the Compost21_GH11. Our results also reveal that MetXyn11 is a monomeric globular-like enzyme with biochemical properties that could be attractive for biotechnological applications, such as: high substrate specificity; wide pH range of activity (pH 5-10) and high pH stability at pH 5-6 (at optimum temperature); high thermal stability at 50 ^{o}C (at optimum pH) for long periods of time; and a unique hydrolytic product release pattern. Indeed, the enzyme exclusively produces xylobiose, which is considered an added-value molecule for various applications. Furthermore, the enzyme addition provoked considerable increase in Cellic CTec3 hydrolysis yields of pretreated sugar cane bagasse, which could be of interest for second generation bioethanol production.

FUNDING

This study was supported by the Fundação de Amparo à Pesquisa do Estado de São Paulo (FAPESP) via grants #10/52362-5, 11/20505-4, 11/21608-1 and 15/13684-0, the Conselho Nacional de Desenvolvimento Científico e Tecnológico (CNPq) via grants # 405191/2015-4, 303988/2016-9, 440977/2016-9 and 151963/2018-5 and the BBSRC of the UK Research and Innovation (grant number: BB/I018492/1).

AUTHORS CONTRIBUTIONS

I.P and D.E.E designed the experiments and wrote the manuscript. D.E.E and V.O.A.P performed MetXyn11 biochemical and biophysical characterization. D.E.E performed the SAXS experiments. M.E.S provided pretreated bagasse samples. I.P., S.M.M., N.C.B., D.E.E. and V.O.A.P. contributed to discussion of the results and editing of the manuscript. All the authors approved the final version.

CONFLICT OF INTEREST

The authors declare that they have no conflict of interest.

COMPLIANCE WITH ETHICAL STANDARDS AND ETHICAL APPROVAL

This article does not contain any studies with human or animal participants.

REFERENCES

Altschul SF, Gish W, Miller W, Myers EW, Lipman DJ (1990) Basic local alignment search tool. J Mol Biol 215:403-410. doi: 10.1016/S0022-2836(05)80360-2

Beaugrand J, Paës G, Reis D, Takahashi M, Debeire P, O'Donoghue M, Chabbert B (2005) Probing the cell wall heterogeneity of micro-dissected wheat caryopsis using both active and inactive forms of a GH11 xylanase. Planta 222:246-257. doi: 10.1007/s00425-005-1538-0

Biely P, Singh S, Puchart V (2016) Towards enzymatic breakdown of complex plant xylan structures: State of the art. Biotechnol Adv 34:1260–1274. doi: 10.1016/j.biotechadv.2016.09.001

Boisset C, Pétrequin C, Chanzy H, Henrissat B, Schülein M (2001) Optimized mixtures of recombinant *Humicola insolens* cellulases for the biodegradation of crystalline cellulose. Biotechnol Bioeng 72:339-345. doi: 10.1002/1097-0290(20010205)72:3<339::AID-BIT11>3.0.CO;2-%23

Camilo C, Polikarpov I (2014) High-throughput cloning, expression and purification of glycoside hydrolases using ligation-independent cloning (LIC). Protein Expr Purif 99:35-42. doi: 10.1016/j.pep.2014.03.008

Cantarel BL, Coutinho PM, Rancurel C, Bernard T, Lombard V, Henrissat B (2009) The Carbohydrate-Active EnZymes database (CAZy): an expert resource for glycogenomics. Nucleic Acids Res 37: D233-D238. doi: 10.1093/nar/gkn663.

Castillo JM, Romero E, Nogales, R (2013) Dynamics of microbial communities related to biochemical parameters during vermicomposting and maturation of agroindustrial lignocellulose wastes. Bioresour Technol 146:345-354. doi: 10.1016/j.biortech.2013.07.093

Curtis TP, Head IM, Graham DW (2003) Theoretical ecology for engineering biology. Environ Sci Technol 37:64A-70A. doi: 10.1021/es0323493

DeLano WL (2002) The PyMOL Molecular Graphics System. Palo Alto, CA, USA.: DeLano Scientific. http://www.pymol.org.

de Oliveira LC, da Silva VM, Colussi F, Cabral AD, de Oliveira Neto M, Squina FM, Garcia W (2015) Conformational changes in a hyperthermostable glycoside hydrolase: enzymatic activity is a consequence of the loop dynamics and protonation balance. PLoS One 10: e0118225. doi: 10.1371/journal.pone.0118225

Duan CJ, Feng JX (2010) Mining metagenomes for novel cellulase genes. Biotechnol Lett 32: 1765-1775. doi: 10.1007/s10529-010-0356-z

Ericsson UB, Hallberg BM, Detitta GT, Dekker N, Nordlund P (2006) Thermofluor-based high-throughput stability optimization of proteins for structural studies. Anal Biochem 357:289-98. doi: 10.1016/j.ab.2006.07.027

Evangelista DE, de Paula FF, Rodrigues A, Henrique-Silva F (2015) Pectinases from *Sphenophorus levis* Vaurie, 1978 (Coleoptera: *Curculionidae*): Putative accessory digestive enzymes. J Insect Sci 15:1536-2442. doi: 10.1093/jisesa/ieu168

Evangelista DE, Kadowaki MAS, Mello BL, Polikarpov I (2018) Biochemical and biophysical characterization of novel GH10 xylanase prospected from a sugar cane bagasse compost-derived microbial consortia. Int J Biol Macromol 109:560-568. doi: 10.1016/j.ijbiomac.2017.12.099

Franke D, Svergun D (2009) DAMMIF, a program for rapid ab-initio shape determination in small-angle scattering. J Appl Crystallogr 42:342-346. doi: 10.1107/S0021889809000338

Ghio S, Ontañon O, Piccinni FE, Díaz de Villegas RM, Talia P, Grasso DH, Campos E (2018) *Paenibacillus* sp. A59 GH10 and GH11 extracellular endoxylanases: Application in biomass bioconversion. BioEnergy Research 11:174–190. doi: 10.1007/s12155-017-9887-7

Guinier A, Fournet G, Walker CB (1995) Small angle scattering of X-rays. Phys Today 9:38-9

Hu J, Davies J, Mok YK, Gene B, Lee QF, Arato C, Saddler JN (2016) Enzymatic hydrolysis of industrial derived xylo-oligomers to monomeric sugars for potential chemical/biofuel production. ACS Sustain Chem Eng 4: 7130-7136. doi: 10.1021/acssuschemeng.6b02008

Isikgor F, Becer C (2015) Lignocellulosic biomass: a sustainable platform for the production of bio-based chemicals and polymers. Polymer Chem 6: 4497-4559. doi: 10.1039/C5PY00263J

Johansson K, El-Ahmad M, Friemann R, Jörnvall H, Markovic O, Eklund H (2002) Crystal structure of plant pectin methylesterase. FEBS Lett 514:243-249. doi: 10.1016/S0014-5793(02)02372-4

Johnson E (2016) Integrated enzyme production lowers the cost of cellulosic ethanol. Biofuels Bioprod Bioref 10:164-174. doi:10.1002/bbb.1634

Kabel MA, den Borne H,Vincken JP, Voragen AGJ, Schols HA (2007) Structural differences of xylans affect their interaction with cellulose. Carbohydrate Polym 69:94-105. doi: 10.1016/j.carbpol.2006.09.006

Kalim B, Böhringer N, Ali N, Schäberle TF (2015) Xylanases–from microbial origin to industrial application. British Biotechnol J 7:1-20. doi: 10.9734/BBJ/2015/15982

Keegstra K (2010) Plant cell walls. Plant Physiol 154:483-486. doi: 10.1104/pp.110.161240

Konarev P, Svergun D (2015) A posteriori determination of the useful data range for small-angle scattering experiments on dilute monodisperse systems. IUCrJ 2:352-360. doi: 10.1107/S2052252515005163

Kont R, Kurašin M, Teugjas H, Väljamäe, P (2013) Strong cellulase inhibitors from the hydrothermal pretreatment of wheat straw. Biotechnol Biofuels 6:135. doi:10.1186/1754-6834-6-135

Kozak M (2006) Solution scattering studies of conformation stability of xylanase XYNII from *Trichoderma longibrachiatum*. Biopolymers 83:95-102. doi: 10.1002/bip.20531

Kozin M, Svergun D (2001) Automated matching of high- and low-resolution structural models. J Appl Crystallogr 34: 33-41. doi: 10.1107/S0021889800014126

Kumar G, Pushpa A, Prabha H (2012) A review on xylooligosaccharides. Int Res J Pharm 3:71-74.

Kumar R, Bhagia S, Smith MD, Petridis L, Ong RG, Cai CM, Mittal A, Himmel MH, Balan V, Dale BE, Ragauskas AJ, Smith JC, Wyman CE (2018) Cellulose–hemicellulose interactions at elevated temperatures increase cellulose recalcitrance to biological conversion. Green Chem 20: 921–934. doi: 10.1039/c7gc03518g

Liao H, Zheng H, Li S, Wei Z, Mei X, Ma H, Shen Q, Xu Y (2015) Functional diversity and properties of multiple xylanases from *Penicillium oxalicum* GZ-2. Sci Rep 5:12631. doi: 10.1038/srep12631.

Lombard V, Golaconda RH, Drula E, Coutinho PM, Henrissat B (2014) The carbohydrate-active enzymes database (CAZy) in 2013. Nucleic Acids Res 42: D490-D495. doi: 10.1093/nar/gkt1178.

Mello BL, Alessi AM, McQueen-Mason S, Bruce NC, Polikarpov I (2016) Nutrient availability shapes the microbial community structure in sugarcane bagasse compost-derived consortia. Sci Rep 6:38781. doi: 10.1038/srep38781

584 Mello BL, Alessi AM, Riaño-Pachón DM, deAzevedo ER, Guimarães FEG, Espirito-Santo MC,
585 McQueen-Mason S, Bruce NC, Polikarpov I (2017) Targeted metatranscriptomics of compost-
586 derived consortia reveals a GH11 exerting an unusual exo-1,4-β-xylanase activity. Biotechnol
587 Biofuels 10:254. doi: 10.1186/s13068-017-0944-4

588 Miller GL (1959) Use of dinitrosalicylic acid reagent for determination of reducing sugar. Anal Chem
589 31:426-428

590 Notredame C, Higgins DG, Heringa J (2000) T-coffee: a novel method for fast and accurate multiple
591 sequence alignment. J Mol Biol 302:205-217. doi: 10.1006/jmbi.2000.4042

592 Paës G, Berrin JG, Beaugrand J (2012) GH11 xylanases: Structure/function/properties relationships and
593 applications. Biotechnol Adv 30:564-592. doi:10.1016/j.biotechadv.2011.10.003

594 Pauchet Y, Wilkinson P, Chauhan R, French-Constant RH (2010) Diversity of beetle genes encoding
595 novel plant cell wall degrading enzymes. PLoS One 5:e15635. doi:
596 10.1371/journal.pone.0015635.

597 Pellegrini VOA, Bernardes A, Rezende CA, Polikarpov I (2018) Cellulose fiber size defines efficiency of
598 enzymatic hydrolysis and impacts degree of synergy between endo- and exoglucanases.
599 Cellulose 25:1865-1881. doi:10.1007/s10570-018-1700-z

600 Petersen TN, Brunak S, von Heijne G, Nielsen H (2011) SignalP 4.0: discriminating signal peptides from
601 transmembrane regions. Nat Methods 8:785-786. doi: 10.1038/nmeth.1701

602 Perry J, Tainer J (2013) Developing advanced X-ray scattering methods combined with crystallography
603 and computation. Methods 59:363-371. doi: 10.1016/j.ymeth.2013.01.005

604 Pollet A, Delcour JA, Courtin CM (2010) Structural determinants of the substrate specificities of
605 xylanases from different glycoside hydrolase families. Crit Rev Biotechnol 30:176-191. doi:
606 10.3109/07388551003645599

607 Polizeli ML, Rizzatti AC, Monti R, Terenzi HF, Jorge JA, Amorim DS (2005) Xylanases from fungi:
608 properties and industrial applications. Appl Microbiol Biotechnol 67:577-591. doi:
609 10.1007/s00253-005-1904-7

610 Rambo RP, Tainer JA (2011) Characterizing flexible and intrinsically unstructured biological
611 macromolecules by SAS using the Porod-Debye law. Biopolymers 95:559-571. doi:
612 10.1002/bip.21638

613 Rittmann BE, Hausner M, Löffler F, Love NG, Muyzer G, Okabe S, Oerther DB, Peccia J, Raskin L,
614 Wagner M (2006) A vista for microbial ecology and environmental biotechnology. Environ Sci
615 Technol 40:1096-103. doi: 10.1021/es062631k

616 Santo ME, Rezende CA, Bernardinelli OD, Pereira N, Curvelo AAS, Deazevedo ER, Guimarães
617 FEG, Polikarpov I (2018) Structural and compositional changes in sugarcane bagasse subjected
618 to hydrothermal and organosolv pretreatments and their impacts on enzymatic hydrolysis. Ind
619 Crop Prod 113:64-74. doi: 10.1016/j.indcrop.2018.01.014

620 Schomburg I, Jeske L, Ulbrich M, Placzek S, Chang A, Schomburg D (2017) The BRENDA enzyme
621 information system-From a database to an expert system. J Biotechnol 261:194-206. doi:
622 10.1016/j.jbiotec.2017.04.020

623 Shi P, Du Y, Yang H, Huang H, Zhang X, Wang Y, Yao B (2015) Molecular characterization of a new
624 alkaline-tolerant xylanase from *Humicola insolens* Y1. Biomed Res Int 2015:149504. doi:
625 10.1155/2015/149504

626 Silva COG, Vaz RP, Filho EXF (2018) Bringing plant cell wall degrading enzymes into the
627 lignocellulosic biorefinery concept. Biofuels Bioprod Bioref 12:277–289. doi:
628 10.1002/bbb.1832

Sims RE, Mabee W, Saddler JN, Taylor M (2010) An overview of second generation biofuel technologies. Bioresour Technol 101:1570-1580. doi: 10.1016/j.biortech.2009.11.046

Slabinski L, Jaroszewski L, Rychlewski L, Wilson IA, Lesley SA, Godzik A (2007) XtalPred: a web server for prediction of protein crystallizability. Bioinform 23:3403-3405. doi: 10.1093/bioinformatics/btm477

Sun FF, Hong J, Hu J, Saddler JN, Fang X, Zhang Z, Shen S (2015) Accessory enzymes influence cellulase hydrolysis of the model substrate and the realistic lignocellulosic biomass. Enzyme Microbial Technol 79:42–48. doi: 10.1016/j.enzmictec.2015.06.020

Suzuki M, Kato A, Nagata N, Komeda Y (2002) A xylanase, AtXyn1, is predominantly expressed in vascular bundles, and four putative xylanase genes were identified in the *Arabidopsis thaliana* genome. Plant Cell Physiol 43:759-767. doi: 10.1093/pcp/pcf088

Svergun DI (1992) Determination of the regularization parameter in indirect-transform methods using perceptual criteria. J Appl Crystallogr 25:495-503. doi: 10.1107/S0021889892001663

Svergun DI, Barberato C, Koch M (1995) CRYSOL - A program to evaluate x-ray solution scattering of biological macromolecules from atomic coordinates. J Appl Crystallogr 28:768-773. doi: 10.1107/S0021889895007047

Väljamäe P, Sild V, Nutt A, Pettersson G, Johansson G (1999) Acid hydrolysis of bacterial cellulose reveals different modes of synergistic action between cellobiohydrolase I and endoglucanase I. Eur J Biochem 266:327-334. doi: 10.1046/j.1432-1327.1999.00853.x

Vázquez MJ, Alonso JL, Domínguez H, Parajó JC (2000). Xylooligosaccharides: manufacture and applications. Trends Food Sci Technol 11:387-393. doi: 10.1016/S0924-2244(01)00031-0

Volkov V, Svergun D (2003) Uniqueness of ab initio shape determination in small-angle scattering. J Appl Crystallogr 36:860-864. doi: 10.1107/S0021889803000268

Walia A, Guleria S, Mehta P, Chauhan A, Parkash J (2017) Microbial xylanases and their industrial application in pulp and paper biobleaching: a review. 3 Biotech 7:11-22. doi: 10.1007/s13205-016-0584-6

Watanabe H, Tokuda G (2001) Animal cellulases. Cell Mol Life Sci 58:1167-78. doi: 10.1007/PL00000931

Wilkins M, Gasteiger E, Bairoch AM, Sanchez JE, Williams K, Appel RD, Hochstrasser D (1999) Protein identification and analysis tools in the ExPASy server. Methods Mol Biol 112:531-552

Yang J, Yan R, Roy A, Xu D, Poisson J, Zhang Y (2015) The I-TASSER Suite: protein structure and function prediction. Nat Methods 12:7-8. doi:10.1038/nmeth.3213

Zhang J, Tuomainen P, Siika-aho M, Viikari L (2011) Comparison of the synergistic action of two thermostable xylanases from GH families 10 and 11 with thermostable cellulases in lignocellulose hydrolysis. Bioresource Technol 102: 9090-9095. doi: 10.1016/j.biortech.2011.06.085

Zhou J, Shi P, Zhang R, Huang H, Meng K, Yang P, Yao B (2011) Symbiotic *Streptomyces sp*. TN119 GH 11 xylanase: a new pH-stable, protease- and SDS-resistant xylanase. J Ind Microbiol Biotechnol 38:523-530. doi: 10.1007/s10295-010-0795-5

671 **Figure Captions**

672 **Fig. 1: Sequences and structures of selected GH11 enzymes.** (A) Multiple alignment between the amino
673 acid sequences from MetXyn11, Compost21_GH11 (PDB id: 5VQJ), and several typical GH11 endo-1,4-
674 β-xylanases (PDB ids: 1XNK, 1H1A, 1XYP, 2JIC and 4XQD). The yellow box shows the extended amino
675 acid sequence present exclusively at the N-terminal of MetXyn11, the red boxes show the two extra loops
676 existent only in MetXyn11 and Compost21_GH11 exo-1,4-β-xylanases. (B) Multiple superposition of the
677 Compost21_GH11 and typical GH11 endo-1,4-β-xylanases crystallographic structures. (C) Superposition
678 of the MetXyn11 3D homology model and the Compost21_GH11crystallographic structure.

679 **Fig. 2: Expression and purification of Xyn11.** SDS-PAGE shows MetXyn11 purification steps; M:
680 molecular mass marker; 0: total soluble protein after IPTG induction; 1: Xyn11 attached to 6xHis-tag, after
681 the first Ni^{+2} affinity chromatography; 2: Xyn11 devoid the fusion 6xHis-tag after the second Ni^{+2} affinity
682 chromatography; 3: final purified Xyn11 after size exclusion chromatography. Size exclusion molecular
683 chromatography shows a unique peak of elution, confirming the sample purity.

684 **Fig. 3: Cleavage pattern of MetXyn11 on heteroxylans**. The cleavage pattern of MetXyn11 was assessed
685 and compared with the cleavage pattern from a typical GH11 endo-1,4-β-xylanase (rGH11XynB).
686 Reactions were performed under the optimal conditions of enzymes for 24 h, using glucuronoxylan and
687 arabinoxylan as substrates. The generated soluble products were analyzed by HPAEC-PAD. (A) and (D):
688 Standards: Solution containing xylooligosaccharides (XOS) from xylose (X_1) to xylohexaose (X_6). (B)
689 Reaction products of rGH11XynB action on glucuronoxylan. (C) Reaction products of MeTXyn11 action
690 on glucuronoxylan. (E) Reaction products of rGH11XynB action on arabinoxylan. (F) Reaction products
691 of MeTXyn11 action on arabinoxylan. The results showed a clear difference between the cleavage patterns
692 of MetXyn11 and rGH11XynB. MetXyn11 releases xylobiose as the only product from both substrates,
693 whereas rGH11XynB generates several other xylooligosaccharides in addition to xylobiose. The results
694 also showed the preference of MetXyn11 for less decorated heteroxylans, since the enzyme liberated much
695 more xylobiose from glucuronoxylan (13% decorated) than arabinoxylan (40% decorated).

696 **Fig. 4: Cleavage pattern of MetXyn11 on xylooligosaccharides.** The MetXyn11 mechanism of action on
697 homoxylan was assessed by HPAEC-PAD analysis, using xylohexaose as a model substrate. Reactions
698 were conducted under the enzyme optimal conditions for 1, 5, 10 and 15 min. A profile of released
699 xylooligossaccharides observed over a period of 15 min shows conversion of xylohexaose in xylotetraose
700 plus xylobiose, and xylotetraose in two xylobioses, besides the conversion of xylopentaose in xylotriose
701 plus xylobiose. Therefore, MetXyn11 cleaves and liberates xylobiose as the only product which is
702 consistent with an exo-catalytic mechanism of the enzyme.

703 **Fig. 5: Thermal and pH stability of MetXyn11.** The thermal stability of MetXyn11 was assessed by both
704 Thermofluor (A-B) and residual activity assays (C-D). In Thermofluor assay, MeTXyn11 was exposed to
705 a wide pH range during a linear increase in temperature until protein thermal denaturation. (A) At the
706 optimal buffer condition (potassium phosphate pH 7.0) MetXyn11 has a T_m of 55 ºC. (B) MetXyn11 has
707 excellent pH stability in a wide range from pH 4 to 10 in ABF buffer. For residual activity assay, MetXyn11
708 activity was measured after keeping the enzyme for 120 h under the optimal conditions for its activity and

also measured after 72 h at optimal temperature (50 ºC), but varying pH from 2 to 10. (C) The enzyme has good thermostability, maintaining 45% of its original activity after 96 h of incubation. (D) MetXyn11 also has good pH stability at pH 5-6 (above 70%).

Fig. 6: Optimal activity conditions and kinetics of MetXyn11. The optimum pH was evaluated in pH range from 2 to 10 in ABF buffer at 50 ºC, while the optimal temperature was assessed in a potassium phosphate buffer at pH 7.0, varying temperature of the experiment from 30 to 70 ºC. MetXyn11 has the highest activity around 50 ºC (A) and pH 6-7 (B). Kinetics experiments revealed a "first-order reaction" profile for MetXyn11 catalytic action even at a high substrate concentration. Kinetic parameters obtained by fitting of this curve resulted in the values of 50.30 $\mu M.s^{-1}$, 121 $mg.mL^{-1}$, 1437 s^{-1} and 11.88 $mL.s^{-1}.mg^{-1}$ for V_{max}, K_M, k_{cat} and $k_{cat}.K_M^{-1}$, respectively.

Fig. 7: Yields of enzymatic hydrolysis of pretreated sugarcane bagasse. Enhancement of commercial enzymatic cocktail Celic CTec3 by addition of MetXyn11 was assessed by HPLC analyses of glucose and xylose under optimal CTec3 conditions of pH and temperature, using hydrothermal pretreated sugarcane bagasse as a substrate. (A) Yield of glucose release as a function of the time using Celic CTec3 alone, and using a mixture of Celic CTec3 plus MetXyn11. (B) The relative increments in the yields of released glucose as a function of the time. (C) Yield of xylose release as a function of the time using Celic CTec3 alone and using a mixture of Celic CTec3 plus MetXyn11. (D) The relative increments in the yields of released xylose as a function of the time.

Fig. 8: SAXS analysis. (A) Experimental solution scattering profile superimposed with the theoretical scattering profile calculated based on MetXyn11 3D homology model. The insert figure shows that the Guinier plot data and the linear regression satisfy the approximation $q < 1.3/R_g$. (B) The p(r) plot displays an almost perfect bell-shape, including an extended tail with a small second peak at the highest q-region, indicating a small deviation of ellipsoidal shape. (C) Porod-Debye plot displays a clear plateau, expected for globular-like proteins that lack disordered regions. (D) The dimensionless Kratky plot presents a well-defined maximum that is consistent with a globular protein, and also presents a subtle elevated baseline at $qR_g > 6$, suggesting some flexibility of the protein structure.

Fig. 9: MetXyn11 low-resolution molecular envelope computed from experimental SAXS data. The 3D-homology model of MetXyn11 (colored) was superposed into the average ab initio SAXS envelope (gray). The N-terminus (N-term) and C-terminus (C-term) of MetXyn11 are indicated for better orientation. The low-resolution envelope fits well the 3D homology model of MetXyn11, revealing a monomeric globular-like protein with a protuberance at its N-terminus.

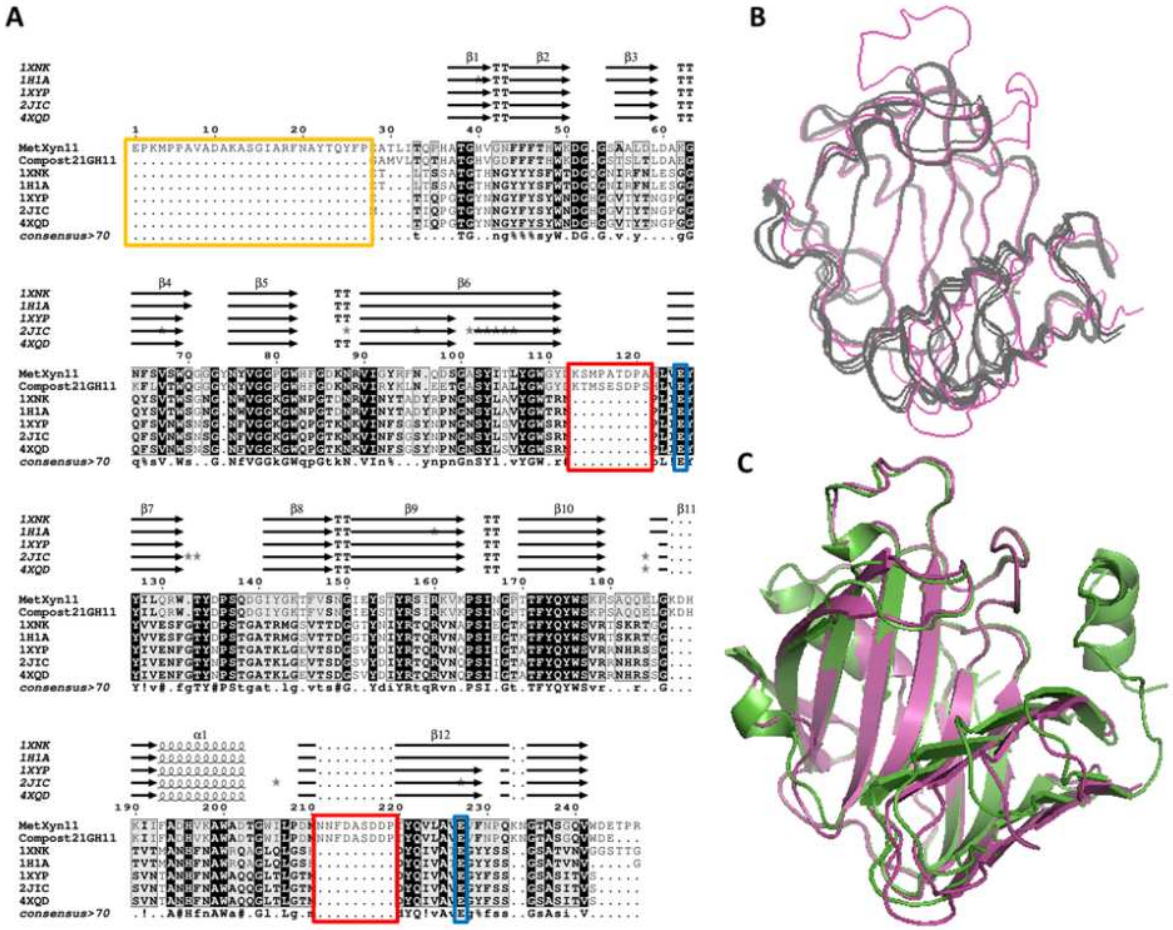

Fig. 1: Sequences and structures of selected GH11 enzymes. (A) Multiple alignment between the amino acid sequences from MetXyn11, Compost21_GH11 (PDB id: 5VQJ), and several typical GH11 endo-1,4-674 β-xylanases (PDB ids: 1XNK, 1H1A, 1XYP, 2JIC and 4XQD). The yellow box shows the extended amino acid sequence present exclusively at the N-terminal of MetXyn11, the red boxes show the two extra loops existent only in MetXyn11 and Compost21_GH11 exo-1,4-β-xylanases. (B) Multiple superposition of the Compost21_GH11 and typical GH11 endo-1,4-β-xylanases crystallographic structures. (C) Superposition of the MetXyn11 3D homology model and the Compost21_GH11crystallographic structure.

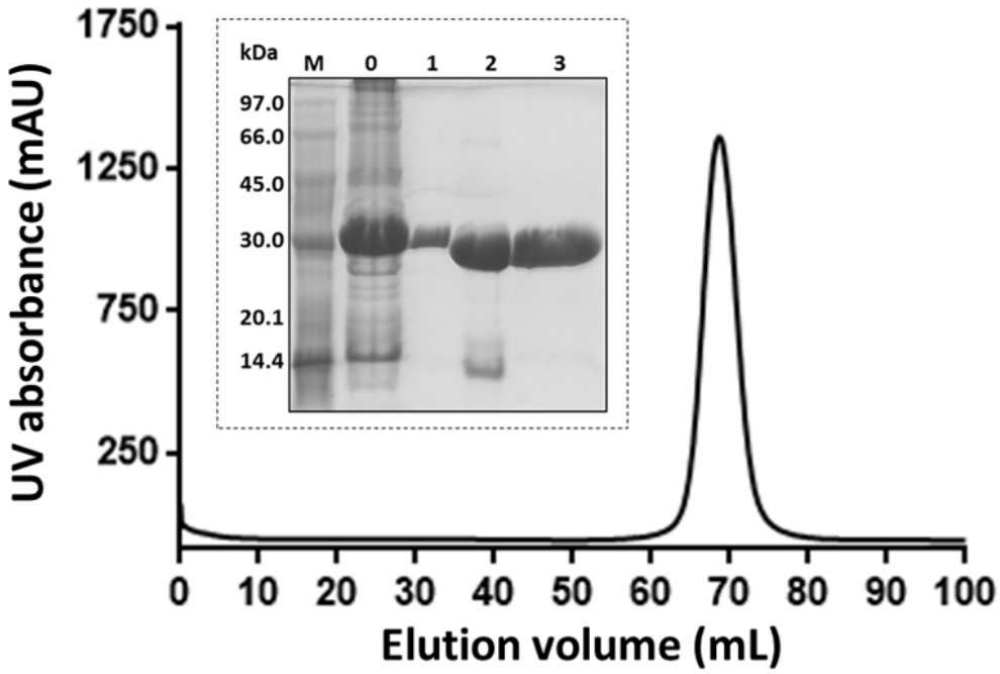

Fig. 2: Expression and purification of Xyn11. SDS-PAGE shows MetXyn11 purification steps; M: molecular mass marker; 0: total soluble protein after IPTG induction; 1: Xyn11 attached to 6xHis-tag, after the first Ni^{+2} affinity chromatography; 2: Xyn11 devoid the fusion 6xHis-tag after the second Ni^{+2} affinity chromatography; 3: final purified Xyn11 after size exclusion chromatography. Size exclusion molecular chromatography shows a unique peak of elution, confirming the sample purity.

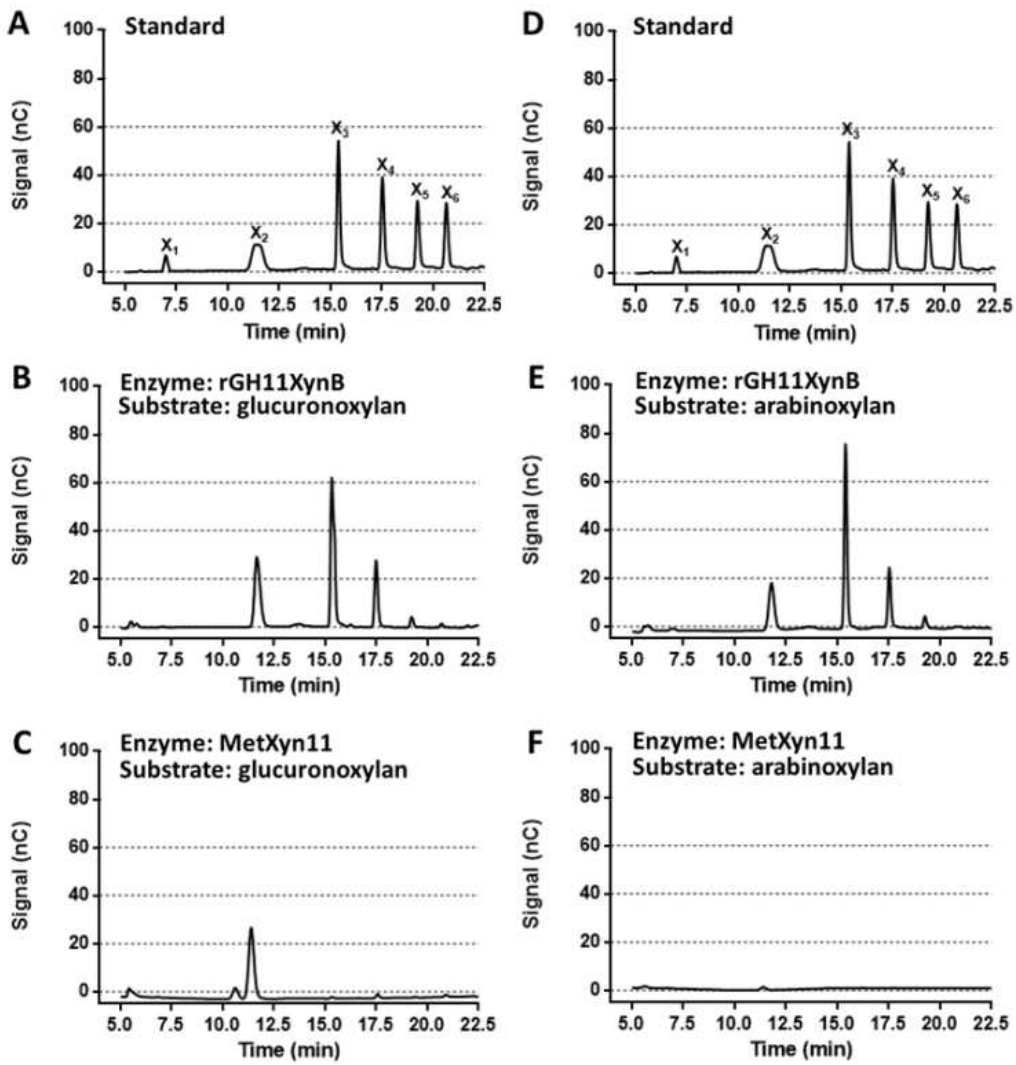

Fig. 3: Cleavage pattern of MetXyn11 on heteroxylans. The cleavage pattern of MetXyn11 was assessed and compared with the cleavage pattern from a typical GH11 endo-1,4-β-xylanase (rGH11XynB). Reactions were performed under the optimal conditions of enzymes for 24 h, using glucuronoxylan and arabinoxylan as substrates. The generated soluble products were analyzed by HPAEC-PAD. (A) and (D): Standards: Solution containing xylooligosaccharides (XOS) from xylose (X_1) to xylohexaose (X_6). (B) Reaction products of rGH11XynB action on glucuronoxylan. (C) Reaction products of MeTXyn11 action on glucuronoxylan. (E) Reaction products of rGH11XynB action on arabinoxylan. (F) Reaction products of MeTXyn11 action on arabinoxylan. The results showed a clear difference between the cleavage patterns of MetXyn11 and rGH11XynB. MetXyn11 releases xylobiose as the only product from both substrates, whereas rGH11XynB generates several other xylooligosaccharides in addition to xylobiose. The results also showed the preference of MetXyn11 for less decorated heteroxylans, since the enzyme liberated much more xylobiose from glucuronoxylan (13% decorated) than arabinoxylan (40% decorated).

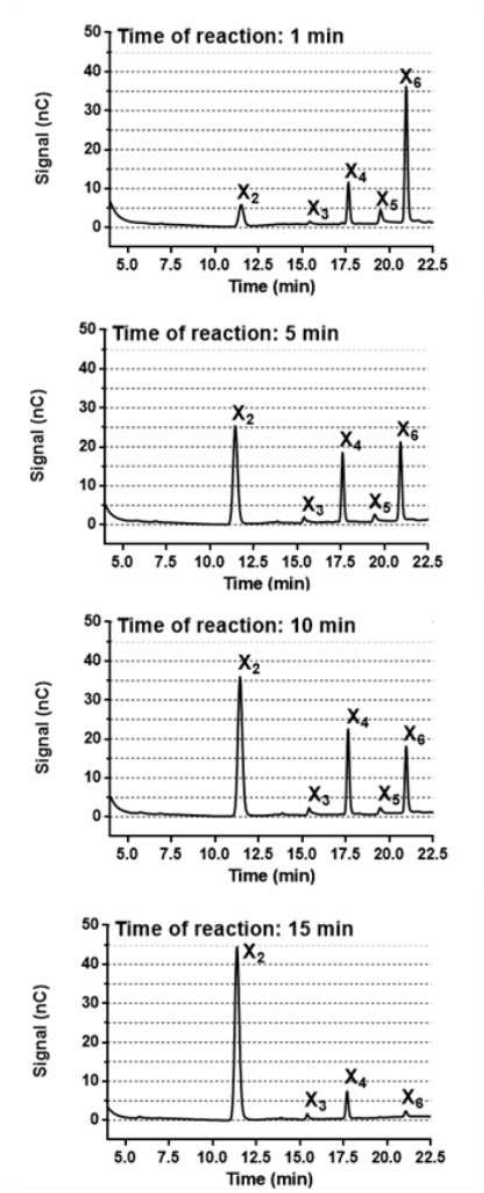

Fig. 4: Cleavage pattern of MetXyn11 on xylooligosaccharides. The MetXyn11 mechanism of action on homoxylan was assessed by HPAEC-PAD analysis, using xylohexaose as a model substrate. Reactions were conducted under the enzyme optimal conditions for 1, 5, 10 and 15 min. A profile of released xylooligossaccharides observed over a period of 15 min shows conversion of xylohexaose in xylotetraose plus xylobiose, and xylotetraose in two xylobioses, besides the conversion of xylopentaose in xylotriose plus xylobiose. Therefore, MetXyn11 cleaves and liberates xylobiose as the only product which is consistent with an exo-catalytic mechanism of the enzyme.

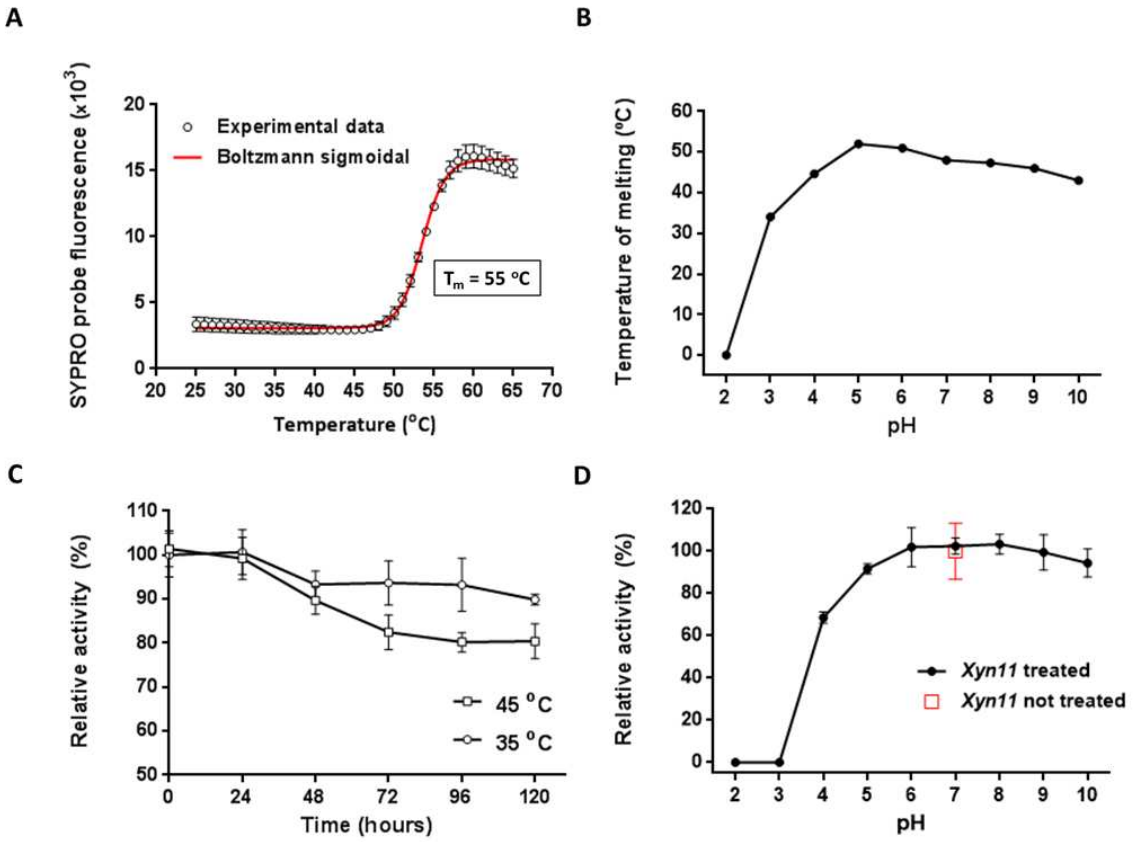

Fig. 5: Thermal and pH stability of MetXyn11. The thermal stability of MetXyn11 was assessed by both Thermofluor (A-B) and residual activity assays (C-D). In Thermofluor assay, MeTXyn11 was exposed to a wide pH range during a linear increase in temperature until protein thermal denaturation. (A) At the optimal buffer condition (potassium phosphate pH 7.0) MetXyn11 has a T_m of 55 ^oC. (B) MetXyn11 has excellent pH stability in a wide range from pH 4 to 10 in ABF buffer. For residual activity assay, MetXyn11 activity was measured after keeping the enzyme for 120 h under the optimal conditions for its activity and also measured after 72 h at optimal temperature (50 ^oC), but varying pH from 2 to 10. (C) The enzyme has good thermostability, maintaining 45% of its original activity after 96 h of incubation. (D) MetXyn11 also has good pH stability at pH 5-6 (above 70%).

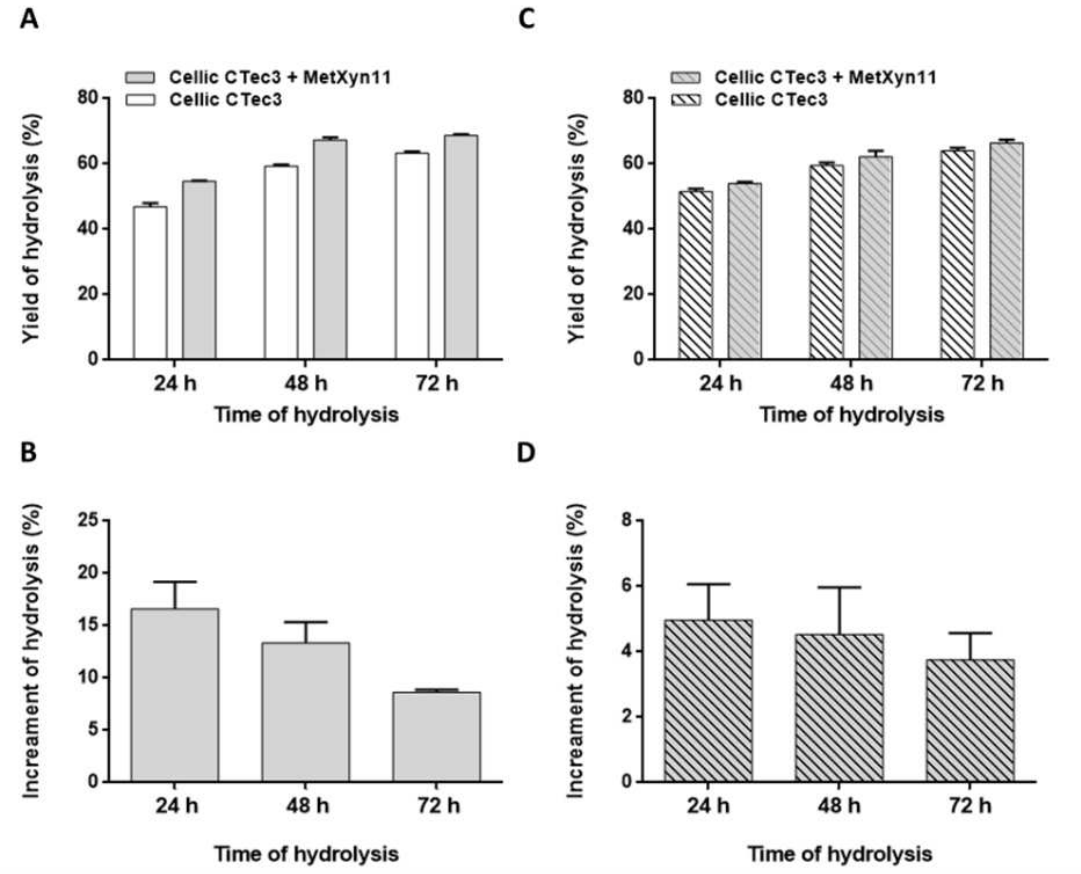

Fig. 7: Yields of enzymatic hydrolysis of pretreated sugarcane bagasse. Enhancement of commercial enzymatic cocktail Celic CTec3 by addition of MetXyn11 was assessed by HPLC analyses of glucose and xylose under optimal CTec3 conditions of pH and temperature, using hydrothermal pretreated sugarcane bagasse as a substrate. (A) Yield of glucose release as a function of the time using Celic CTec3 alone, and using a mixture of Celic CTec3 plus MetXyn11. (B) The relative increments in the yields of released glucose as a function of the time. (C) Yield of xylose release as a function of the time using Celic CTec3 alone and using a mixture of Celic CTec3 plus MetXyn11. (D) The relative increments in the yields of released xylose as a function of the time.

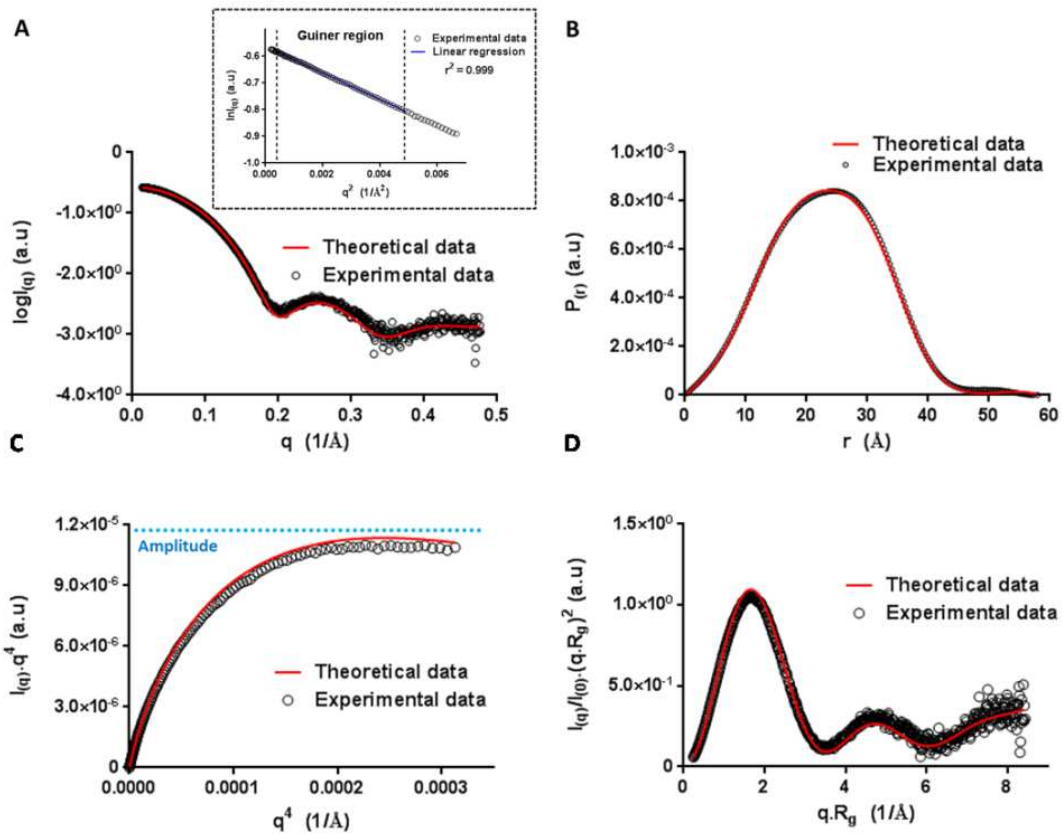

Fig. 8: SAXS analysis. (A) Experimental solution scattering profile superimposed with the theoretical scattering profile calculated based on MetXyn11 3D homology model. The insert figure shows that the Guinier plot data and the linear regression satisfy the approximation $q < 1.3/R_g$. (B) The p(r) plot displays an almost perfect bell-shape, including an extended tail with a small second peak at the highest q-region, indicating a small deviation of ellipsoidal shape. (C) Porod-Debye plot displays a clear plateau, expected for globular-like proteins that lack disordered regions. (D) The dimensionless Kratky plot presents a well-defined maximum that is consistent with a globular protein, and also presents a subtle elevated baseline at $qR_g > 6$, suggesting some flexibility of the protein structure.

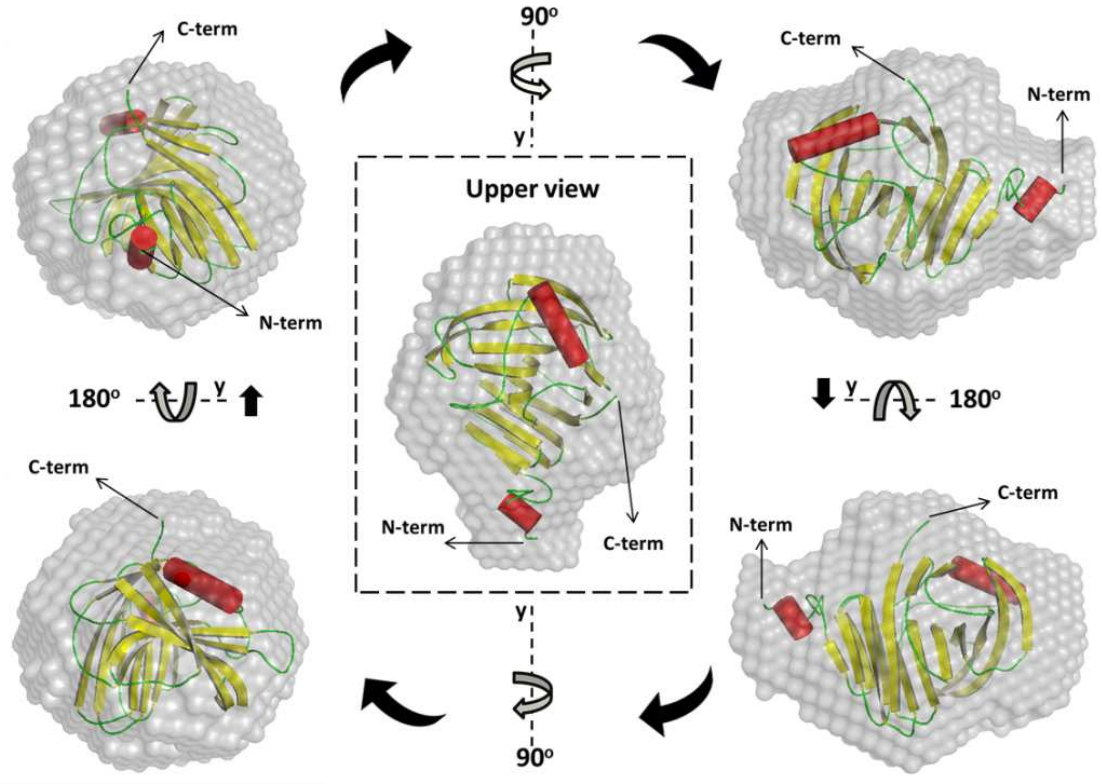

Fig. 9: MetXyn11 low-resolution molecular envelope computed from experimental SAXS data. The 3D-homology model of MetXyn11 (colored) was superposed into the average ab initio SAXS envelope (gray). The N-terminus (N-term) and C-terminus (C-term) of MetXyn11 are indicated for better orientation. The low-resolution envelope fits well the 3D homology model of MetXyn11, revealing a monomeric globular-like protein with a protuberance at its N-terminus.

Applied Microbiology and Biotechnology

Supplementary Materials

Biochemical characterization and low-resolution SAXS shape of a novel GH11 exo-1,4-β-xylanase identified in a microbial consortium

Danilo Elton Evangelista[1a], Vanessa de Oliveira Arnoldi Pellegrini[1a], Melissa Espirito Santo[1], Simon McQueen-Mason[2], Neil C. Bruce[2] and Igor Polikarpov[1*].

[1]Instituto de Física de São Carlos, Universidade de São Paulo, Avenida Trabalhador Sãocarlense 400, 13566-590 São Carlos – SP, Brazil.

[2]Department of Biology, University of York, Wentworth Way, York, UK, YO10 5DD

[a]These authors contributed equally to this work

*Corresponding author: ipolikarpov@ifsc.usp.br , tel.: +55(16)3373-8088; fax: +55(16) 3373-9881

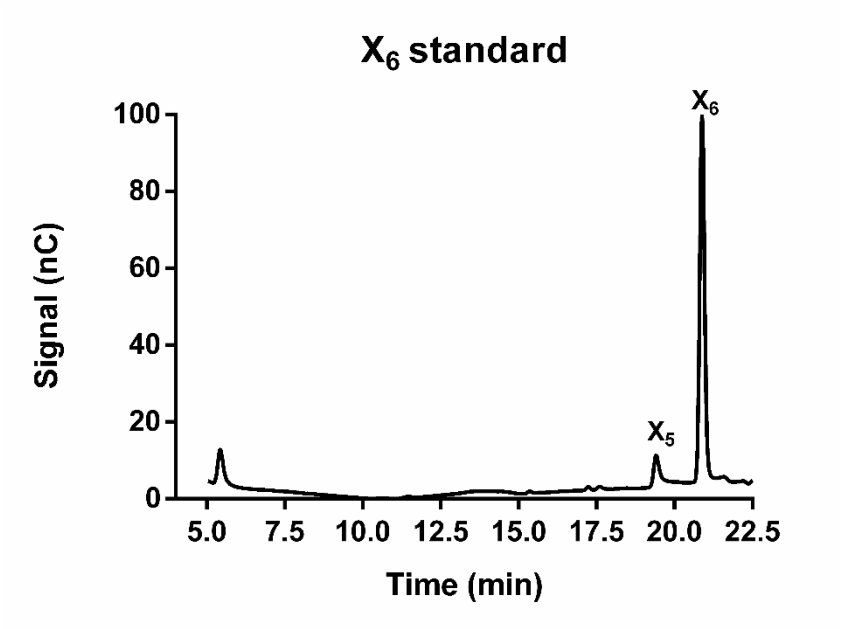

Figure S1. HPAEC-PAD analysis of xylohexaose (X6) standard. Small contamination with xylopentaose (X5) can be clearly visualized.

Table S1. Thermofluor analysis. Effect of different buffer solutions on tertiary structure stability of MetXyn11. Asterisk indicates the highest T_m values.

pH	Buffer (50 mM)	T_m (°C)
7.0	Control (water)	55*
1.2	HCl	26
2.0	HCl	45
3.0	Citric acid	26
4.0	Sodium citrate	46
4.5	Sodium acetate	48
4.7	Sodium citrate	51
5.0	Sodium acetate	52
5.0	Potassium phosphate	54
5.5	Sodium citrate	54
5.5	Sodium phosphate	55*
5.8	MES	55
6.0	Potassium phosphate	54
6.0	Bis-Tris	55*
6.2	MES	55*
6.5	Sodium phosphate	53
6.5	Sodium cacodylate	54
6.5	Bis-Tris	55*
6.5	MES	55*

6.7	Bis-Tris	55*
7.0	Potassium phosphate	53
7.0	HEPES	55*
7.0	Bis-Tris	55*
7.3	Amonium acetate	54
7.5	Sodium phosphate	50
7.5	Tris	54
8.0	Imidazole	52
8.0	HEPES	52
8.0	Tris	52
8.0	Bicine	52
8.5	Tris	51
9.0	Bicine	49
9.5	Sodium carbonate	46
10.0	Sodium carbonate	45

Table S2. Metal ions and chemicals influence. The effects of the metal ions, reducing agents and surfactants on MetXyn11 enzymatic performance were assessed and compared with other GH11 xylanases. N/A = Not available.

Enzyme name	MetXyn11	Xyn11A	Xyn11B	Xyn11B119
Organism	Unknown	*P. oxalicum*	*P. oxalicum*	*Streptomyces sp.*
Reference	Present study	Liao et al. 2015	Liao et al. 2015	Zhou et al., 2011
Metal ions		**Residual activity (%)**		
	(10 mM)	(10 mM)	(10 mM)	(10 mM)
Control	100.0 ± 1.8	100.0 ± 3.7	100.0 ± 0.6	100.0 ± 2.6
Ca^{+2}	81.3 ± 4.2	118.9 ± 1.7	100.1± 3.4	98.3 ± 5.1
Co^{+2}	79.0 ± 6.8	124.9 ± 2.5	81.7 ± 1.6	97.3 ± 2.8
Cu^{+2}	54.3 ± 1.7	2.3 ± 0.16	41.6 ± 2.6	N/A
Fe^{+2}	53.6 ± 3.5	115.5 ± 3.1	101.3 ± 2.5	101.0 ± 1.6
Fe^{+3}	0.50 ± 0.7	22.8 ± 1.0	33.0 ± 0.5	N/A
Mn^{+2}	21.9 ± 10.3	108.8 ± 2.8	100.1 ± 2.7	65.6 ± 0.9
Mg^{+2}	123.1 ± 6.9	127.6 ± 2.0	101.8 ± 2.7	99.0 ± 0.8
Ni^{+2}	110.2 ± 1.6	116.1 ± 2.5	79.1 ± 3.1	122.3 ± 2.8
K^{+}	112.3 ± 10.3	N/A	N/A	101.4 ± 2.6
Li^{+2}	106.1 ± 6.35	119.4 ± 2.3	89.6 ± 3.9	101.3 ± 3.6
Reducing agents		**Residual activity (%)**		
	(1 mM)	(1 mM)	(1 mM)	(10 mM)
β-Mercaptoethanol	84.8 ± 0.9	41.7 ± 0.1	101.0 ± 5.3	126.5 ± 2.0
DTT	95.1 ± 1.7	100.2 ± 1.2	98.3 ± 2.6	N/A
Surfactants		**Residual activity (%)**		
	(0.1%)	(0.1%)	(0.1%)	(0.3%)
Tween-20	83.5 ± 0.3	100.8 ± 1.2	104.6 ± 7.6	N/A
Triton-100X	107.9 ± 0.4	100.0 ± 1.1	88.8 ± 2.9	N/A
SDS	0.0 ± 0.0	23.9 ± 1.8	3.5 ± 0.3	110.8 ± 7.2

Table S3. SAXS data collection and processing.

Data collection	
Beamline	LNLS-SAXS1
Wavelength (Å)	1.55
q range ($Å^{-1}$)	0.0138 – 0.47699
Exposure time per frame (s)	30
Concentration range ($mg.mL^{-1}$)	1.0, 3.5 and 15.0
Temperature (°C)	20
Data Analysis	
$I_{(0)}$	0.26 ± 0.00
Guinier q-region ($Å^{-1}$)	0.0138 – 0.06983
R_g (Å) from Guinier (± SE)	18.52 ± 0.04
R_g (Å) from GNOM (± SE)	17.67 ± 0.06
D_{max} (Å)	58
Resolution ($2\pi.q_{max}^{-1}$) (Å)	13.17
Oligomeric state	Monomer
Ab initio modeling	
Number of models	10
NSD	0.572 ± 0.008
Software employed	
Primary data reduction	Fit2D
Data processing	Primus
Theoretical data fitting	Crysol
Envelope modeling	Dammin
3D-Homology modeling	I-Tasser